

Inferring solid-state diffusivity in lithium-ion battery active materials: improving upon the classical GITT method

A. Emir Gümriükçüoğlu,¹ James Burridge,¹ Kieran O'Regan,² and Jamie M. Foster^{1,3}

¹*School of Mathematics and Physics, University of Portsmouth, Lion Terrace, Portsmouth PO1 3HF, UK*

²*About:Energy, Labs Camden - Atrium The Stables Market, Chalk Farm Road, London, England, NW1 8A*

³*The Faraday Institution, Quad One, Becquerel Avenue, Harwell Campus, Didcot, OX11 0RA, UK*

(Dated: April 26, 2024)

The Galvanostatic Intermittent Titration Technique (GITT) is a ubiquitous method for determining the solid-state diffusivity in lithium-ion battery materials. However, it is notoriously time-consuming and relies upon assumptions whose applicability is questionable. We propose a novel methodology that allows inference of the diffusivity for a more general class of data that is simpler and faster to harvest. We infer the diffusivity (as a function of stoichiometry) by minimising the residual sum of squares between data and solutions to a spherically-symmetric diffusion model in a single representative active material particle. Using data harvested from the NMC cathode of a commercial LG M50 cell we first demonstrate that our method is able to reproduce the diffusivities inferred by the GITT, which requires ten days of galvanostatic intermittent titration data. We then demonstrate that our method reliably reconstructs diffusivity using significantly less data. Despite arising from quick-to-measure data, our method more accurately infers diffusivities. This work is a contribution towards developing faster and more reliable techniques in parameter inference for lithium-ion batteries.

I. INTRODUCTION

The Doyle-Fuller-Newman (DFN) model [1–4] is widely acknowledged as the gold standard in physics-based modelling for lithium-ion batteries and offers a framework for understanding and predicting device behaviour at the level of individual and electrode pairs. Provided that the parameterisation has been performed accurately, the DFN model has been shown to reliably predict the electrochemical response of real batteries in realistic operating conditions; with observed and predicted voltages often matching to within a single percentage [5–8]. So ubiquitous is the DFN model that a wealth of literature exists on various model simplifications and extensions, many of which are discussed in a recent review by Brosa Planella et. al [9]. One prevalent class of simplified DFN models are the so-called single particle models (SPM) [10–13]. These are generally accurate for low and moderate C-rate operating (<1C, or thereabouts), in which all the particles in each electrode behave similarly and so the model can be reduced to that of lithium transport within one “representative” particle in each electrode. The distribution of lithium ions within these representative particles are assumed to obey a spherically-symmetric diffusion process.

As alluded to above, the predictive power of the DFN, and related physics-based models, is predicated upon knowledge of parameters that cannot be directly measured but must instead be inferred through physical principles and indirect experimental observations. Therefore, the process of parameterisation – the accurate inference of these parameters – is crucial for developing effective battery models, which in turn are key to advancing device improvement and control [14].

One of the most influential parameters in physics-based models (especially SPMs) is the solid state diffusivity of lithium-ions within the active materials, $D(c)$, which varies (often rather strongly) with concentration c , and must be inferred. The most widespread inference approach is to collect data with the Galvanostatic Intermittent Titration Technique (GITT), where the electrode is forced with a small constant current for a short time, then allowed to relax until the lithium ions are fully diffused, with the forcing–relaxation cycle repeated until the state-of-charge range of interest is covered. This technique allows each forcing–relaxation cycle to be analysed separately as an independent diffusion problem with constant diffusivity and homogeneous initial concentration. Using the analytic solution of a semi-infinite slab (or, the *Sand equation* [15]), one can determine a diffusion constant corresponding to the small range of concentrations in the cycle [16].

Despite its widespread application, the GITT approach presents several limitations, with one of the most prominent being the practical challenge of data collection. For typical particle sizes $R \sim \mathcal{O}(1)\mu\text{m}$ and diffusion constants $D \sim \mathcal{O}(10^{-15})\text{m}^2/\text{s}$, the constant current should be applied for $\mathcal{O}(10)$ seconds to accurately determine $D(c)$. As a consequence, in order to adequately reconstruct $D(c)$ across the relevant range of concentrations, it is necessary to apply low currents several hundred times. Each pulse is followed by a relaxation period, typically lasting around an hour, to restore uniform concentration, a prerequisite for applying the Sand equation to the next pulse. Thus the total data collection time can span weeks. A second type of issue is that of the questionable embedded assumptions. The GITT inference is carried out using a solution that pertains for semi-infinite slabs, yet the models in which the

parameters will be used contain diffusion equations in a sphere. Thus there is inconsistency in between inference and prediction. The semi-infinite slab approximation is appropriate for pulse durations t_{pulse} much shorter than the diffusion time scale $t_d = R^2/D$. The accuracy decreases as the ratio t_{pulse}/t_d increases, with a 5% deviation from the spherical solution at $t_{\text{pulse}}/t_d \approx 3 \times 10^{-2}$ [17]. For $t_{\text{pulse}} > 0.04 t_d$, the Sand equation becomes inadequate for determining $D(c)$ (a detailed discussion is presented in Appendix A).

In addition to the GITT, other techniques to determine the diffusivity exist. Cyclic voltammetry allows estimation of the average (constant) diffusivity [18, 19]; electrochemical impedance spectroscopy [20]; the potentiostatic intermittent titration technique [21]; the intermittent current interruption technique [22].

In this paper, we propose determining the diffusivity by *inference from spherical diffusion model* (ISDM). In the spirit of SPMs, we solve the fully nonlinear spherical diffusion model in a single representative particle for a known surface lithium flux (directly proportional to the known current applied to/drawn from the cell) and determine the concentration at the particle surface. Via the equilibrium overpotential, $U_{\text{eq}}(c)$, we calculate the cell voltage, $V(t)$, and by comparing this quantity to the observed cell voltage, we infer $D(c)$. In contrast with the GITT, our approach offers the following benefits: (i) it can be applied to data with *any* current profile as long as the concentration spans the range of state of charge of interest, thereby allowing for very significantly reduced data collection times; (ii) the model being used for inference is compatible with those in which the parameters will subsequently be used to make predictions, thus there are no embedded assumptions and it is therefore valid for all diffusion timescales; (iii) as we will show the parameters inferred by ISDM may offer improved predictive capability for many use cases of interest. To validate our approach, we use half-cell data harvested from a commercial LG M50 NMC811 cathode from Ref. [23] and show that by using data covering a significantly shorter time, we are able to match, and arguably improve upon, the parameter inference produced by the GITT. The remainder of this paper is organised as follows. In Section II, we outline the mathematical method underlying ISDM. We validate our approach in Section III using both synthetic and experimental data for GITT current profiles. In Section IV we demonstrate the generality of our approach by inferring diffusivity from experimental data generated by applying a constant current. We then compare ISDM to the GITT in recovering a known diffusivity in a full DFN model simulation data in Section V. We conclude with Section VI where we summarise and discuss our results.

II. THE ISDM APPROACH

In this section we present the system of equations (reminiscent of a SPM) that lie at the heart of the ISDM. We then discuss the details of the inference approach before moving onto validation in Section III.

For the present study, our aim is to write down the simplest physics-based model that contains only the parameters that one infers with the GITT, thereby ensuring an even playing field in terms of what we are expecting to learn from ISDM vs. GITT. If confronted with data where the influence of other parameters are nonnegligible, then our ISDM methodology remains robust once one the inference model is extended to include those parameters concurrently with diffusivity.

A. A single particle model

We consider a representative particle with radius R , where the molar Li ion concentration $c(t, r)$ on the sphere follows the radially symmetric diffusion equation

$$\frac{\partial c}{\partial t} = \frac{1}{r^2} \frac{\partial}{\partial r} \left(r^2 D(c) \frac{\partial c}{\partial r} \right), \quad (1)$$

subject to the initial condition

$$c(0, r) = c_0, \quad (2)$$

and boundary conditions

$$\left. \frac{\partial c}{\partial r} \right|_{r=0} = 0, \quad -D(c) \left. \frac{\partial c}{\partial r} \right|_{r=R} = j, \quad (3)$$

where $j(t)$ is the molar surface flux, describing the rate of Li ions transferred across the particle's surface. Under the usual SPM assumption that the dynamics of each particle are very similar, we can (to a good approximation)

apportion the current applied to/drawn from the cell, $I(t)$, equally between particles, such that

$$j = \pm \frac{I}{F n 4 \pi R^2}, \quad (4)$$

where n is the number of active particles in the electrode, and $F = e N_A = 9.6485 \times 10^4 \text{C/mol}$ is Faraday's constant. The sign above is negative for the cathode and positive for the anode, so that positive values of $I(t)$ correspond to a lithiating cathode (and delithiating anode) and hence battery discharging.

In most experiments, one applies $I(t)$ and measures the voltage $V(t)$. Neglecting the reaction overpotential and internal resistance, the dominant contribution to the voltage comes from the equilibrium potential, that is,

$$V = U_{\text{eq}}(c_{\text{surf}}), \quad (5)$$

where $c_{\text{surf}}(t) = c(t, R)$ is the surface concentration of Li ions.

B. Inference of diffusivity and the parameterisation scheme

Let $\mathcal{D} = \{t_i, I_i, V_i\}_{i=1}^N$ be an experimental data and let us assume that the particle number n , radius R and $U_{\text{eq}}(c)$ are known from independent measurements. In order to infer concentration-dependent diffusivity, we parameterise it as $D(c; \theta)$, where θ is the parameter vector.

The spatial derivatives in Eq. (1) are treated using the conservative control-volume method [24] thereby reducing the PDE to a system of coupled ODEs for the concentrations at given collocation points, r_i , as functions of time only. We proceed to numerically solve the ODE system for given parameters θ . Using the solution on the particle surface $c(t, R; \theta)$, we define the loss function as the mean of the residual sum of squares:

$$\mathcal{L}(\theta) = \frac{1}{N} \sum_{i=1}^N (V_i - U_{\text{eq}}(c(t_i, R; \theta)))^2. \quad (6)$$

The parameters θ can be estimated by minimising the loss:

$$\hat{\theta} = \underset{\theta}{\operatorname{argmin}} \mathcal{L}(\theta), \quad (7)$$

which is equivalent to a maximum likelihood estimate under the assumption of Gaussian errors.

The main challenge in this approach is the parameterisation of $D(c)$. To model diffusivity, there exists an infinite number of choices of functional forms. Parameterisations with few number of parameters generally do not reflect the complexity of the GITT estimation. On the other hand, increasing the number of parameters leads to a high dimensional parameter space which makes it impractical to scan for a global minimum of the loss function.

In this proof-of-principle study, we model $D(c)$ as a piecewise linear function, where the \mathcal{N} dimensional parameter vector θ is defined as the array of diffusivity values at predetermined knots. To estimate these parameters, we first bin the time series data into \mathcal{N} partitions. Each partition α has the corresponding data:

$$\mathcal{D}_\alpha = \{t_{\alpha i}, I_{\alpha i}, V_{\alpha i}\}_{i=1}^{N_\alpha}, \quad (8)$$

where N_α is the number of data points in partition $\alpha \in \{1, \dots, \mathcal{N}\}$. We evolve the diffusion equation for each partition sequentially, assuming a series of Fickian diffusion processes with constant diffusivity θ_α in each segment, and solve the corresponding optimisation problem. Defining the local loss in partition α as

$$\mathcal{L}_\alpha(\theta_\alpha) = \frac{1}{N_\alpha} \sum_{i=1}^{N_\alpha} [V_{\alpha i} - U_{\text{eq}}(c(t_{\alpha i}, R; \theta_\alpha))]^2, \quad (9)$$

we estimate the constant diffusivity θ_α as

$$\hat{\theta}_\alpha = \underset{\theta_\alpha}{\operatorname{argmin}} \mathcal{L}_\alpha(\theta_\alpha). \quad (10)$$

The value of the corresponding knot \hat{c}_α is defined by evolving the diffusion equation for the partition using the estimated diffusivity $\hat{\theta}_\alpha$ and averaging it over time and volume:

$$\hat{c}_\alpha = \frac{3}{T_\alpha R^3} \int_0^R \int_{t_{\alpha 1}}^{t_{\alpha 1} + T_\alpha} r^2 c(t, r; \hat{\theta}_\alpha) dt dr, \quad (11)$$

where T_α is the duration of the evolution that falls into partition α . At the end of this procedure, we obtain \mathcal{N} pairs of $(\hat{c}_\alpha, \hat{\theta}_\alpha)$ values which can be seen as sample points from the full diffusivity function $D(c)$ that is most likely to produce the experimental data in each partition.

It should be noted that this approach is not a comprehensive optimisation strategy in the global sense. For scenarios in which the concentration gradients within the particle are minimal, e.g. a galvanostatic intermittent titration (GIT) experiment with slow constant charge input and frequent relaxation periods, the local optimisation procedure yields highly precise outcomes. On the other hand, for cases with high overlap in c values across partitions, it is necessary to transition to a more global optimisation scheme. In this study, this transition is accomplished by our second optimisation phase, where $D(c; \theta)$ is initialised as a piecewise linear function with knots $(\hat{c}_\alpha, \hat{\theta}_\alpha)$ obtained in the first phase; the values of $\hat{\theta}_\alpha$ are then improved towards the minimum of the global (or quasi-global) loss function using a numerical gradient algorithm. The updated parameter values are then used to construct the final inferred function $\hat{D}(c) = D(c; \hat{\theta})$. The pseudocode for our two-stage optimisation approach is presented in Appendix B.

For the success of the first (local) optimisation stage, the selection of the number and locations of the partitions is a crucial step. The optimum choice heavily relies on the form of input current and the density of data, such that each partition contains sufficient information about the diffusion of Li ions. For instance, a typical GIT experiment consists mostly of stabilisation data, where the potential does not noticeably change; these data points contain minimal information once the relaxation is well under way. For the specific example of GIT data, a natural choice is to select the partitions such that they each coincide with at least one pulse and relaxation period to democratically distribute the diffusion information across the partitions. On the other hand, for an experiment where there is no obvious choice for partitioning, e.g. a battery sourced by a continuous constant current (see Section IV), one option is to bin the data such that each partition contains an equal amount of *useful* data points, which we define as points where the change in voltage ΔV is above a certain pre-set threshold value ΔV_{\min} .¹

The parameterisation and optimisation schemes adopted in this study are only a subset of possible approaches for ISDM. For materials with well-characterised diffusion properties, adopting a physics-informed parameterisation will closely align the model with the underlying physical principles, while reducing the number of inferred parameters θ significantly. Additionally, the adjoint sensitivity method, which facilitates an effective use of gradient descent variants, can be adopted as an alternative optimisation strategy. For the present study, where a major focus is a GIT experiment with very large number of data points, a global parameterisation with adjoint methods proves to be computationally expensive and can become unstable due to the complexity of the diffusion equation. Instead, the two-stage approach adopted here allows us to analyse individual segments of data separately with parameters localised in each segment, providing a more practical application of ISDM in this initial study.

III. VALIDATION

In this Section, we show that ISDM produces a diffusivity that is consistent with the one obtained with the GITT. For the purposes of demonstration we will use a commercially relevant cathode comprised of NMC811. The measurements have already been reported in Ref. [23]. In the interests of brevity we refer the interested reader to [23] with a brief summary of the data collection method given below.

The data contains four cycles: the first one (cycle 0) is a charging cycle with constant current for about 10 hours, followed by (cycle 1) a discharge cycle of the same duration, but opposite current. Then there is a GIT charge cycle (cycle 2) consisting of 249 periods of constant pulse (150 seconds) and relaxation (1 hour). The last part of the data is a GIT discharge cycle (cycle 3) with the same parameters for 250 periods, with an opposite-sign current. For this experiment, a 15 mm diameter and 75.6 μm thickness coin cell is used, and the constant current for all cycles is $I = 0.78$ mA (or $C/10$). The average particle radius is $R = 5.22$ μm . The delithiation starts at minimum state of charge with fully diffused concentration $c = 0.9084 c_{\max}$. Maximum concentration is reported as $c_{\max} = 51765$ mol/m³ [23].

In this section, we establish the diffusivity derived from the conventional GITT procedure, denoted as D_{GITT} , as the baseline diffusivity for comparison with the ISDM results. We calculate D_{GITT} by applying the Sand equation to each forcing-relaxation period within the GIT charging data.

¹ If the current direction remains the same throughout the experiment, an alternative would be to define the partitions such that the transferred electric charge is uniformly distributed across the partitions.

A. Self-Validation

We start by demonstrating the efficacy of the ISDM method in accurately reproducing diffusivity. We generate synthetic data by solving the spherical diffusion equation for a particle using $D_{\text{GIT}}(c)$ and $U_{\text{eq}}(c)$, both obtained from the conventional GITT approach. The diffusion equation is forced by the same current time series in the GIT charging data, with 249 periods of pulse and relaxation.

We note that this self-validation step focusses solely on the performance of the ISDM method and is not influenced by the validity of the semi-infinite slab approximation or the suitability of the spherical diffusion model for this context; within the scope of this synthetic data analysis, the $D_{\text{GIT}}(c)$ function is treated as the “true” diffusivity.

We divide the synthetic data into $\mathcal{N} = 50$ partitions, such that each partition contains 5 whole GIT periods, with the last one covering 4. For the first stage of the optimisation, we create a uniform grid with 10 points for $\log_{10} \left(\frac{10^{15}}{\text{m}^2/\text{s}} D \right)$ within the range $[-2, 2]$. We evaluate the loss at these points to identify the minimum. If a minimum is located, the range encompassed by the grid point and its two adjacent points is subdivided into 10 finer points, and this process is repeated until desired accuracy is reached. If no minimum is found within this range, the number of grid points is expanded by a factor of 10, and the range is extended by 1 unit on both sides. As a result we obtain 50 pairs of $(\hat{c}_\alpha, \hat{\theta}_\alpha)$.

The second stage of the optimisation scheme is intended to change the inferred diffusivity towards the minimum of the *global* loss. To this goal, we adopt a variant of cyclic coordinate descent algorithm. We construct the stepwise linear $D(c; \theta)$ function with parameters θ initialised at the estimates $\hat{\theta}$ from the previous step. For the GIT data, there is minimal overlap in concentration across the partitions; the slow forcing and relaxation periods prevent the growth of c gradients. We therefore employ a quasi-global loss function for each partition, defined as:

$$\mathcal{L}_\alpha^{(\beta)}(\theta_\alpha) = \frac{1}{\sum_{i=\alpha-\beta}^{\alpha+\beta} N_i} \sum_{i=\alpha-\beta}^{\alpha+\beta} \sum_{j=1}^{N_i} [V_{i,j} - U_{\text{eq}}(c(t_{i,j}, R; \theta_\alpha))]^2, \quad (12)$$

where β is the number of neighbours (left and right) for each partition α . For inference from synthetic data we use $\beta = 2$, that is, for each θ_α parameter, we include 5 partitions to calculate the quasi-global loss (12). We then estimate the gradient of $\mathcal{L}_\alpha^{(\beta)}(\theta_\alpha)$ with respect to θ_α numerically and update the values of $\hat{\theta}_\alpha$, sequentially going over each partition. We repeat this procedure until the global loss $\mathcal{L}(\theta)$ converges and we obtain our final $\hat{D}(c) = D(c; \hat{\theta})$ from ISDM.

The results of ISDM procedure is shown in Fig.1 for $\mathcal{N} = 50$ partitions, along with the “true” value $D_{\text{GIT}}(c)$ which was used to generate the synthetic data. In the plot, we also show $\tilde{D}_{\text{GIT}}(c)$ which is obtained by applying the traditional GITT to this synthetic data for comparison. For the synthetic data, the ISDM result $\hat{D}(c)$ is in good agreement with the original $D_{\text{GIT}}(c)$ used to generate the data.

To quantify the accuracy of the predictions from our model, we first note that an overwhelming portion of the data is determined by the correct choice of the equilibrium potential $U_{\text{eq}}(c)$. Therefore we expect the predictions to be very close to the data. Instead of directly quantifying how much of the data is explained, we instead quantify how much of the data *in excess of a null model* can be predicted by the model. To this end, we choose a null model corresponding to $D(c) \rightarrow \infty$, which predicts instantaneous diffusion, i.e.

$$V^{\text{null}}(t) = U_{\text{eq}}(c_{\text{av}}(t)), \quad (13)$$

where $c_{\text{av}}(t)$ is the average concentration across the particle at time t , and U_{eq} is determined from the relaxation values in the GITT forcing-relaxation data. Defining the voltage data in excess of the null model as

$$\Delta V_i = V_i - V^{\text{null}}(t_i), \quad (14)$$

the predicted voltage deviation from the null model for a given $D(c)$ is

$$\Delta V_i^{\text{pred}}(D) = U_{\text{eq}}(c_{\text{pred}}(t_i, R; D)) - V^{\text{null}}(t_i), \quad (15)$$

where $c_{\text{pred}}(t, R; D)$ is the concentration predicted by the specific $D(c)$ model used.

We define the coefficient of determination R^2 as the proportion of variability in the dataset beyond that explained by the null model, accounted for by a spherical diffusion model with diffusivity $D(c)$. Specifically,

$$R^2(D) = 1 - \frac{\sum_{i=1}^N \left(\Delta V_i - \Delta V_i^{\text{pred}}(D) \right)^2}{\sum_{i=1}^N \left(\Delta V_i - \frac{1}{N} \sum_{j=1}^N \Delta V_j \right)^2}. \quad (16)$$

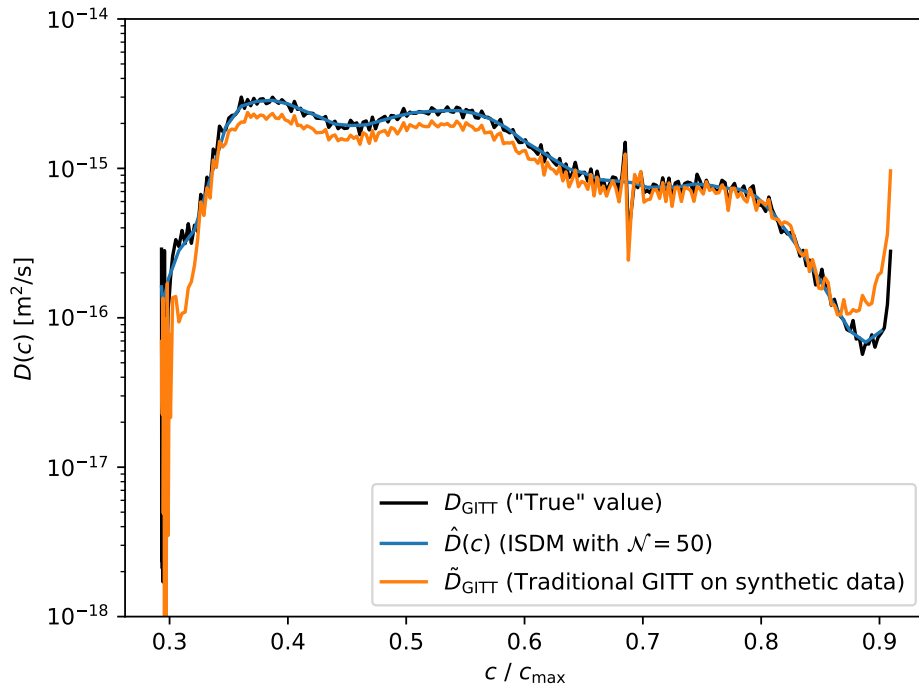


FIG. 1. The diffusivity inferred from a synthetic data using ISDM on 50 partitions. The current is chosen to coincide with the GIT charge cycle in [23]. The solid black line shows the *true* value of $D(c)$ used to generate the synthetic data, while the solid blue line is the result of applying the traditional GITT on the synthetic data.

Note that $R^2 \in (-\infty, 1]$, where 1 indicates a perfect fit, values close to 0 suggest that the model does not improve upon the null model, and negative values reveal that the model adds more variability than the null model. The coefficient of determination for the ISDM estimate $\hat{D}(c)$ is calculated as follows:

$$R^2(\hat{D}) = 0.997, \quad (17)$$

that is, ISDM yields a model that can account for almost all the variability in the data. For comparison we apply the traditional GITT, using the Sand equation on the synthetic data to infer the diffusivity $\tilde{D}_{\text{GITT}}(c)$. This model produces less accurate predictions compared to ISDM, with $R^2(\tilde{D}_{\text{GITT}}) = 0.800$.

Since the true diffusivity is known for the synthetic data, we can also define a measure of accuracy for $D(c)$ itself:

$$R_D^2(D) = 1 - \frac{\langle (D(c) - D_{\text{true}})^2 \rangle_c}{\langle (D_{\text{true}}(c) - \langle D_{\text{true}}(c) \rangle_c)^2 \rangle_c}, \quad (18)$$

where $\langle f(c) \rangle_c$ denotes the mean of a function $f(c)$ over the range of c .² The metric R_D^2 quantifies the proximity of the estimated diffusivity to its true value. For the ISDM estimate, we calculate

$$R_D^2(\hat{D}) = 0.991, \quad (19)$$

while using the diffusivity obtained by applying the traditional GITT to the synthetic data, we get $R^2(\tilde{D}_{\text{GITT}}) = 0.882$.

This demonstrates the self-consistency of our approach. Since the synthetic data was generated from a single particle spherical diffusion model, it is no surprise that the spherical-diffusion-based ISDM performs better than GITT, which is based on semi-infinite slab approximation.

² It is important to note that this measure loses significance if D_{true} is flat, i.e. does not exhibit variations. Nevertheless, for the cases examined in this paper, the diffusivities typically have strong dependence on concentration and R_D^2 proves to be a reliable metric for assessing the differences of the inferred diffusivities from the true one.

B. Validation with real data

After confirming that the ISDM approach can reproduce the true $D(c)$ from synthetic data, we move on to analysing the real data from Ref.[23]. Specifically, we consider the GIT charging cycle from which we inferred $D_{\text{GIT}}(c)$ in the previous sub-section using the conventional GITT. We note that the $U_{\text{eq}}(c)$ function used in this section is also inferred from the GIT data.

After applying the partitioning and optimisation scheme outlined in section III A, we obtain the ISDM result for diffusivity. In Fig.2, we show the inferred $\hat{D}(c)$ for 50 partitions.

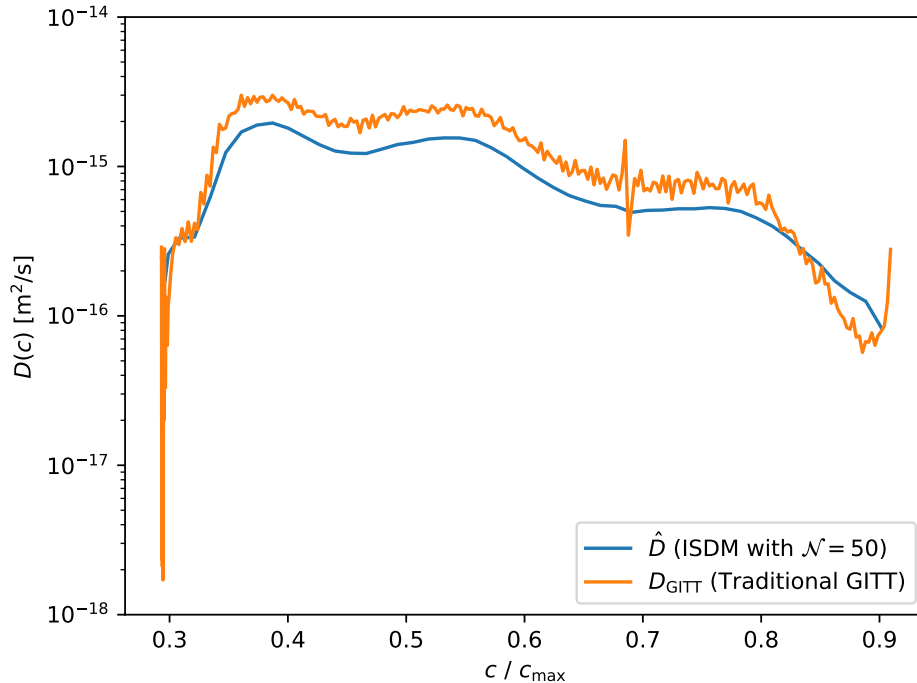


FIG. 2. The diffusivity inferred from real GIT charging data using ISDM on 50 partitions. We also show $D_{\text{GIT}}(c)$ obtained with the conventional GITT, i.e. by applying the Sand equation to each GIT period in the data.

The coefficient of determination, as defined in Eq.(16), for the ISDM result is computed as

$$R^2(\hat{D}) = 0.501, \quad (20)$$

that is, the predictive model accounts for half of the deviations in the data from the null model. On the other hand, using D_{GIT} , i.e. the diffusivity obtained by applying the Sand equation, this quantity is slightly lower, with $R^2(D_{\text{GIT}}) = 0.470$.

Interestingly, ISDM estimates a diffusivity $\hat{D}(c)$ that is generally lower than the conventional GITT result D_{GIT} . The mean relative deviation is 48%. We show the plot for the percentage relative deviations for all available c values in Figure.3 We see that the typical relative deviation is of order $\mathcal{O}(10)\%$. The largest contribution arises from the marginal values of concentration. Constraining the comparison to $c \in [0.3, 0.9]$, the mean relative percentage deviation drops down to 34%. In Appendix A, we showed how the GITT result suffers from errors due to approximating the spherical particle with a semi-infinite slab, which would render the ISDM result more accurate. On the other hand, the GITT is insensitive to constant contributions to the output voltage during the pulse regime, such as internal resistance effects.

IV. INFERENCE WITH CONSTANT CURRENT PROFILE

So far, our application of ISDM has been limited to GIT data, serving mainly for comparison with the traditional GITT-based methods. On the other hand, the true strength of ISDM lies in its versatility to infer diffusivity across the range of concentration spanned by *any* current profile.

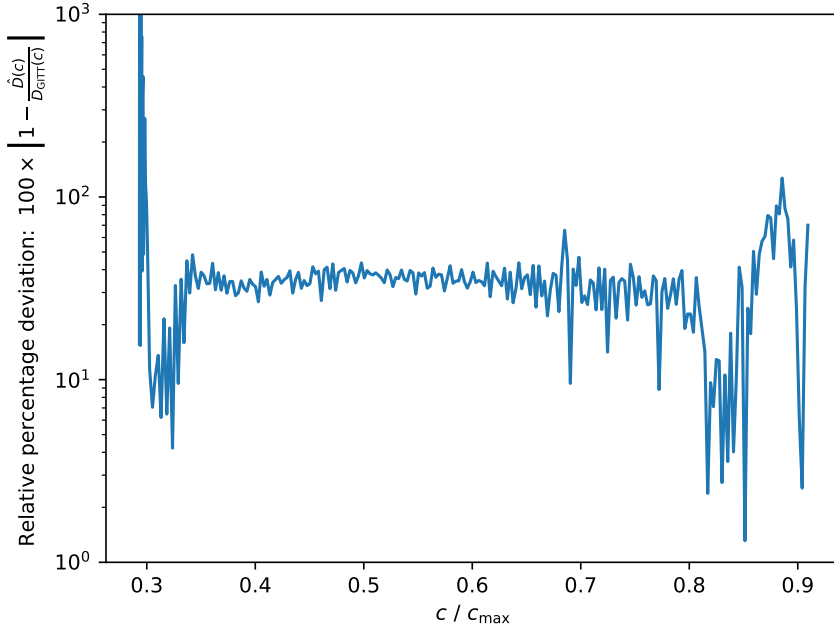


FIG. 3. The relative percentage deviation of the ISDM result $\hat{D}(c)$ with respect to $D_{\text{GITT}}(c)$, both estimates inferred from the same GIT charge data.

In this section, we consider the constant current measurements of Chen et al [23] and use ISDM to estimate $D(c)$. The data contains a 10-hour measurement where the electrode is charged with a constant $C/10$ current.

A vital component of our inference methodology is the equilibrium potential $U_{\text{eq}}(c)$, which, until now, has been derived from GIT data. For ISDM to be used as a swift alternative to the GITT, it becomes essential to determine $U_{\text{eq}}(c)$ without resorting to the extensive, weeks-long measurements traditionally required. In this section, we perform ISDM using two different equilibrium potentials: $U_{\text{eq}}^{(\text{GITT})}(c)$ obtained from GIT data and $U_{\text{eq}}^{(\text{pOCV})}(c)$ obtained from $C/20$ charge/discharge data. The latter data set [25] was acquired from a half cell cathode and consists of alternating charge and discharge cycles, repeated 10 times. We estimate $U_{\text{eq}}^{(\text{pOCV})}(c)$ as outlined in Appendix C, averaging over the 10 charge/discharge cycles.

For partitioning, we distribute the *useful* data evenly into 50 partitions. We define a useful data where the change in output voltage between two consecutive points exceeds $2 \times 10^{-4} \text{V}$.

The first stage of optimisation is performed as prescribed in Sec. III A, allowing us to obtain constant diffusion values θ_α for each partition, corresponding to the average concentrations \hat{c}_α . For the second stage, the quasi-global loss definition is no longer useful, since the constant current introduces nonnegligible gradients across the particles and the parameters θ_α are no longer localised to their corresponding partitions. We therefore use a traditional gradient descent algorithm where we use the global loss function (6) and numerically estimate the gradients with respect to every parameter θ_α , then update all parameters simultaneously towards the minimum of the global loss until convergence.

We show the results in Figure.4 for inference from $C/10$ charging data, compared with the corresponding GITT result, using both choices of the equilibrium potential. The coefficients of determination for the two case are calculated as:

$$\begin{aligned} R^2(\hat{D}) &= 0.863, & \left(\text{using } U_{\text{eq}}^{(\text{GITT})} \right), \\ R^2(\hat{D}) &= 0.860, & \left(\text{using } U_{\text{eq}}^{(\text{pOCV})} \right). \end{aligned} \quad (21)$$

where for the computation of model predictions, we use the corresponding $U_{\text{eq}}(c)$ that was used when inferring each $\hat{D}(c)$. For comparison, the traditional GITT result gives $R^2(D_{\text{GITT}}) = 0.0017$ (using $U_{\text{eq}}^{(\text{GITT})}$).

The poor performance of D_{GITT} in explaining the constant charge data underlines the inconsistency between the predictive model (single particle spherical diffusion) and the inference data model (single particle slab diffusion), which

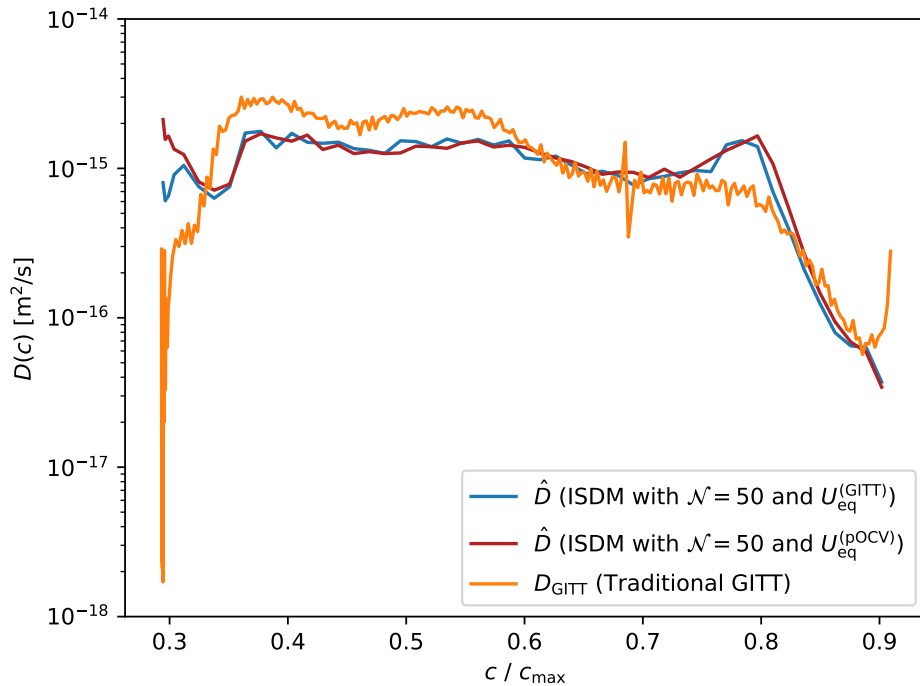


FIG. 4. The diffusivity $D(c)$ inferred from ISDM on real $C/10$ charging data of Ref.[23], using 50 partitions. The blue and red plots lines correspond to $\hat{D}(c)$ inferred using $U_{\text{eq}}(c)$ from GITT and pOCV, respectively. The orange line represents the diffusivity obtained with the conventional GITT.

becomes particularly apparent when the system is subjected to a more generalised forcing beyond the periodic pulse-relaxation signal.

V. ACCURACY COMPARISON: ISDM VS GITT

In Sections III B and IV, we have demonstrated that ISDM outperforms the traditional GITT in explaining the data. However, these assessments are primarily consistency tests that hinge on the validity of the single-particle approximation. Moreover, we have neglected any contribution from e.g. overpotentials, electrolyte. Given these constraints, the superior data fitting of ISDM compared to the GITT is expected, as ISDM is specifically designed to minimise deviations from observed data it is inferred from. Nonetheless, neither analysis provides insight into which of the inferred diffusivities is more correct. Even in Section III A, where the true diffusivity was known, the synthetic data originated from a single-particle model, limiting the analysis therein to only a self-consistency test.

To fairly compare the results of ISDM and the GITT, we require an unbiased data with a known diffusivity. To this end, we used Dandelion [26] for DFN model simulations of a LG M50 NMC811 cathode half-cell with various current profiles, using the parameters from Ref.[23]. In these runs, we use a realistic diffusion function formulated as the exponential of a high-order polynomial, whose full form can be retrieved from the links provided in footnotes 3–5. The equilibrium potential was fixed to be the fitted function presented in Ref.[23].

We first generate a dataset for a cathode half-cell charging with a GIT forcing-relaxation current ³ (covering 9.5 days of data). We then apply the traditional GITT with Sand equation to determine diffusivity $D_{\text{GITT}}(c)$.

We then move on to applying ISDM to the simulated half-cell, which consists of two stages. In the first stage we apply charge then discharge the half-cell with a constant $C/20$ current ⁴ (covering 40 hours of data), which allows us to determine $U_{\text{eq}}^{(\text{pOCV})}$ as described in Appendix C. In the second stage, we generate charging data with $C/10$

³ The Dandelion run for GIT pulse-relaxation current can be accessed at:

<https://simulation.dandelion.com/legacy/simulation/?id=40751b48-307b-46fb-bcb9-5b3ab79b3b5c>

⁴ The Dandelion run for charge and discharge with constant $C/20$ current can be accessed at:

<https://simulation.dandelion.com/legacy/simulation/?id=d91db0e5-e0bb-4391-936c-50c69f267c24>

constant current ⁵ (covering 10 hours) and apply ISDM (with $\mathcal{N} = 50$ partitions) to infer diffusivity $\hat{D}(c)$, using the equilibrium potential $U_{\text{eq}}^{\text{(pOCV)}}$.

The comparison of the inferred diffusivities along with the true one is shown in Fig.5. Coefficient of determination

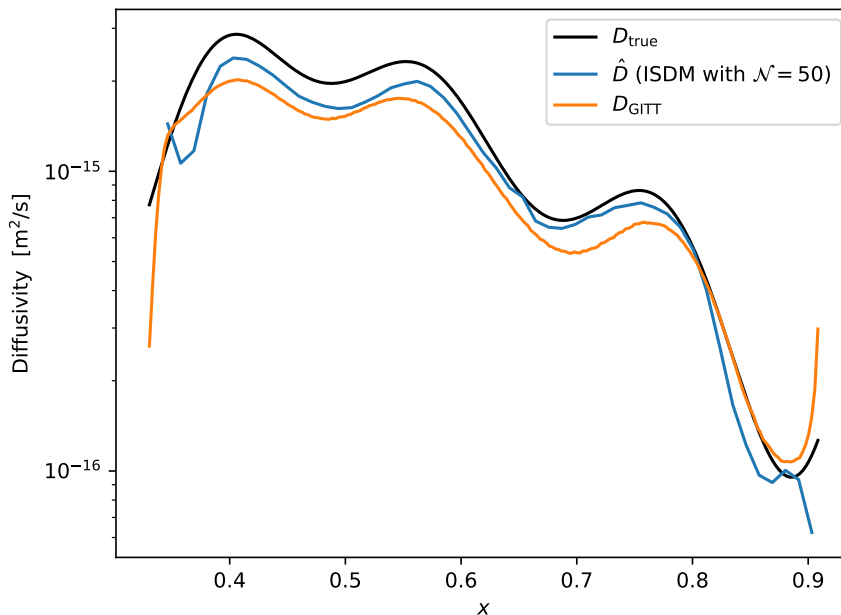


FIG. 5. Comparison of diffusivities inferred using ISDM (\hat{D}) with 50 partitions and the traditional GITT (D_{GITT}), along with the true value used to generate the DFN data.

for diffusivity R_D^2 , defined in Eq.(18), which quantifies how close the inferred functions are to the true diffusivity is calculated for each case as:

$$R_D^2(\hat{D}) = 0.883, \quad R_D^2(D_{\text{GITT}}) = 0.777. \quad (22)$$

ISDM not only achieves a more accurate approximation of the true diffusivity compared to GITT, but it also requires only 50 hours of data collection, in contrast to the 9.5 days necessary for GITT. This represents a 78% reduction in data collection time.

VI. CONCLUSIONS

We have introduced a novel methodology for inferring the concentration-dependent solid-state diffusivity using experimentally measured voltage data. We refer to our method as “inference from spherical diffusion model” (ISDM). The ISDM approach offers advantages over the GITT, namely: (i) it does not depend upon the questionable semi-infinite slab assumption inherent in the Sand equation, (ii) it does not require a carefully controlled pulsed current input and lengthy relaxation intervals. The proposed approach is highly versatile, and can infer diffusivity from any current excitation which causes the concentration to pass through the desired range of values, and which is consistent with the assumptions of the SPM. This allows significant savings in experimental time.

We first showed that ISDM is capable of recovering the correct diffusivity from synthetic data (generated by solving the model equations forward with a known diffusivity). This demonstrates that ISDM is consistent, in contrast to the GITT. Second, we applied the approach to real galvanostatic intermittent titration (GIT) data from an LG M50 NMC811 cathode [23]. The diffusivity inferred by our method is in good agreement with the results of the GITT.

⁵ The Dandelion run for charging with constant $C/10$ current can be accessed at:
<https://simulation.dandelion.com/legacy/simulation/?id=3865ded1-60e1-439b-82b3-65a0ec8c5b0c>

Third, we applied ISDM to C/10 galvanostatic charging data, which is much faster and easier to harvest than GIT data. Once again, we were able to obtain results broadly consistent with the diffusivity inferred from the previous tests. Finally, we directly compared the performance of ISDM and the GITT at inferring diffusivity. We used the DFN model to generate synthetic GIT charge, C/20 charge-discharge and C/10 charge data using a realistic pre-specified diffusivity. Diffusivities were then predicted from this data using both the GITT and ISDM, with the latter method producing substantially more accurate results.

The most obvious application for our method is in inferring the diffusivity of an electrode at the beginning of life in order to make predictions of the device behaviour in the future. However, owing to the speed and agility of the technique it may prove useful in other ways. It is well-known that degradation, for example in the form of microscale intra-particle cracks, causes the effective diffusivity of the insertion material to reduce with cycle number. Since the ISDM is agnostic to data-type, it could be used in the field to update the model parameters from incoming data as the devices ages, maintaining the predictive capability of the model. These parameter changes might also be used as an advanced indicator of approaching device failure or nonlinear ageing. Finally, we emphasise that although we have chosen to focus on solid-state diffusivity there are no conceptual hurdles to applying the technique elsewhere. In Li-ion batteries it could be used to infer electrolytic conductivity, transference number, or activation energies for the Arrhenius temperature dependence of the diffusivity. It may also prove useful in a variety of other energy capture and storage devices.

ACKNOWLEDGMENTS

We are grateful to Edmund Dickinson for their invaluable comments and suggestions on an earlier version of the draft. JF was supported by the Faraday Institution Multi-Scale Modelling (MSM) project Grant number EP/S003053/1.

Appendix A: Validity of Slab approximation on a sphere

In this appendix, we discuss the validity of the slab approximation implicit in Sand equation to describe a spherical diffusion process. Similar analyses was presented in Ref.[17] and in the Supplementary Information of Ref.[22]. In particular, we quantify the validity of $D(c)$ obtained using the Sand equation on an actual galvanostatic intermittent titration (GIT) experiment.

We consider the spherical diffusion equation (1) for constant diffusivity D , forced with a constant surface flux j_0 , and starting with an initial homogenous concentration c_0 . We rescale concentration c , distance r and time t with initial concentration c_0 , particle radius R and diffusion timescale t_d , respectively. That is,

$$\tilde{c}(t, r) = \frac{c(t, r)}{c_0}, \quad x = \frac{r}{R}, \quad \tau = \frac{t}{t_d} = \frac{Dt}{R^2}. \quad (\text{A1})$$

With these redefinitions, Eq.(1) becomes

$$\frac{\partial \tilde{c}(\tau, x)}{\partial \tau} = \frac{\partial^2 \tilde{c}(\tau, x)}{\partial x^2} + \frac{2}{x} \frac{\partial \tilde{c}(\tau, x)}{\partial x}, \quad (\text{A2})$$

subject to:

$$\tilde{c}(0, x) = 1, \quad \left. \frac{\partial \tilde{c}(\tau, x)}{\partial x} \right|_{x=0} = 0, \quad \left. \frac{\partial \tilde{c}(\tau, x)}{\partial x} \right|_{x=1} = -\delta, \quad (\text{A3})$$

where we defined

$$\delta = \frac{j_0 R}{c_0 D}. \quad (\text{A4})$$

The solution to Eq.(A2) is known analytically [27, 28],

$$\tilde{c}(\tau, x) = 1 - \delta \left[3\tau + \frac{5x^2 - 3}{10} - \frac{2}{x} \sum_{n=1}^{\infty} \frac{\sin(\alpha_n x)}{\alpha_n^2 \sin(\alpha_n)} e^{-\alpha_n^2 \tau} \right], \quad (\text{A5})$$

where α_n is the n -th positive root of the transcendental equation $\alpha = \tan \alpha$.

On the surface ($x = 1$), this solution reduces to:

$$\tilde{c}(\tau, 1) = 1 - \delta \left[3\tau + \frac{1}{5} - 2 \sum_{n=1}^{\infty} \frac{e^{-\alpha_n^2 \tau}}{\alpha_n^2} \right]. \quad (\text{A6})$$

At $\tau = 0$, the sum evaluates to $\sum_{n=1}^{\infty} \alpha_n^{-2} = 1/10$ [29], which verifies the initial condition $\tilde{c}(0, 1) = 1$.

One way to determine the behaviour of the finite sum is to approximate it into an integral. We observing that for large n , the recursion approximates to $\alpha_{n+1} \approx \alpha_n + \pi$. Extending this relation, we have

$$\alpha_n \approx \alpha_1 + (n-1)\pi, \quad (\text{A7})$$

which is accurate at 1% level for low n , but becomes more precise for larger values. This allows the approximation

$$S = \sum_{n=1}^{\infty} \frac{e^{-\alpha_n^2 \tau}}{\alpha_n^2} \approx \sum_{n=1}^{\infty} s(n), \quad (\text{A8})$$

where we defined

$$s(n) = \frac{e^{-[\alpha_1 + (n-1)\pi]^2 \tau}}{[\alpha_1 + (n-1)\pi]^2}. \quad (\text{A9})$$

Next, we approximate the infinite sum (A8) with the Euler-Maclaurin formula:

$$S = \sum_{n=1}^{\infty} s(n) \approx \int_1^{\infty} s(x) dx + \frac{s(\infty) + s(1)}{2} + \sum_{k=1}^{\infty} \frac{B_{2k}}{(2k)!} \left(s^{(2k-1)}(\infty) - s^{(2k-1)}(1) \right), \quad (\text{A10})$$

where B_{2k} are the even Bernoulli numbers. Since we are only interested in small τ approximation, we only keep terms up to linear order in τ . The integral is straightforward to evaluate and we find:

$$\int_1^{\infty} s(x) dx = \frac{e^{-\alpha_1^2 \tau}}{\alpha_1 \pi} - \sqrt{\frac{\tau}{\pi}} \operatorname{erfc}(\alpha_1 \sqrt{\tau}) = \frac{1}{\alpha_1 \pi} - \sqrt{\frac{\tau}{\pi}} + \mathcal{O}(\tau) \quad (\text{A11})$$

As for the correction terms, $s(n)$ and its odd derivatives evaluated at infinity all vanish. The only remaining contributions come from the function and its derivatives at $n = 1$. The infinite sum of odd derivatives at $n = 1$ are problematic. Around $k = 12$ th term, the sum starts to grow rapidly. On the other hand, these terms only give contributions at order τ^0 , τ^2 and higher. Since we are only interested in the behaviour of the $\tau^{1/2}$ term, we will assume that these terms can be resummed. Considering the finite limit for $\tau \rightarrow 0$, we conjecture that

$$S \approx \frac{1}{10} - \sqrt{\frac{\tau}{\pi}} + \mathcal{O}(\tau). \quad (\text{A12})$$

That is, for small τ , the solution to the spherical diffusion equation is approximated as

$$\frac{\tilde{c}(\tau, 1) - 1}{\delta} = -2 \sqrt{\frac{\tau}{\pi}} + \mathcal{O}(\tau). \quad (\text{A13})$$

Written in dimensionful quantities, the surface concentration is:

$$c_{\text{surf}} = c_0 - 2j_0 \sqrt{\frac{t}{D\pi}} + \mathcal{O}\left(\frac{Dt}{R^2}\right). \quad (\text{A14})$$

Thus, for $t \ll R^2/D$, the spherical diffusion equation has the same surface solution as the diffusion equation for a semi-infinite slab [16] which forms the basis of the Sand equation. Although Eq.(A14) suggests that the GITT would be applicable for short pulses, we need to determine how small Dt/R^2 should be to determine the diffusivity reliably using the GITT.

Moreover, at relatively large τ , the infinite sum decays exponentially, and we are left with

$$\frac{\tilde{c}(\tau, 1) - 1}{\delta} = -\frac{1}{5} - 3\tau, \quad (\text{A15})$$

or

$$c_{\text{surf}} = c_0 - \frac{j_0 R}{D} \left(\frac{1}{5} + \frac{3tD}{R^2} \right), \quad (t \sim R^2/D). \quad (\text{A16})$$

This expression is particularly interesting since the surface concentration depends linearly on t and the slope is independent of D . Therefore if one employs the GITT in this regime, the inferred diffusion constants will be arbitrary. Again, we need to use numerical methods to determine precisely the time $\tau = tD/R^2$ where this behaviour becomes relevant.

In Figure 6, we show a comparison of the full solution and demonstrate the validity of (A13) and (A15) in the corresponding regimes.

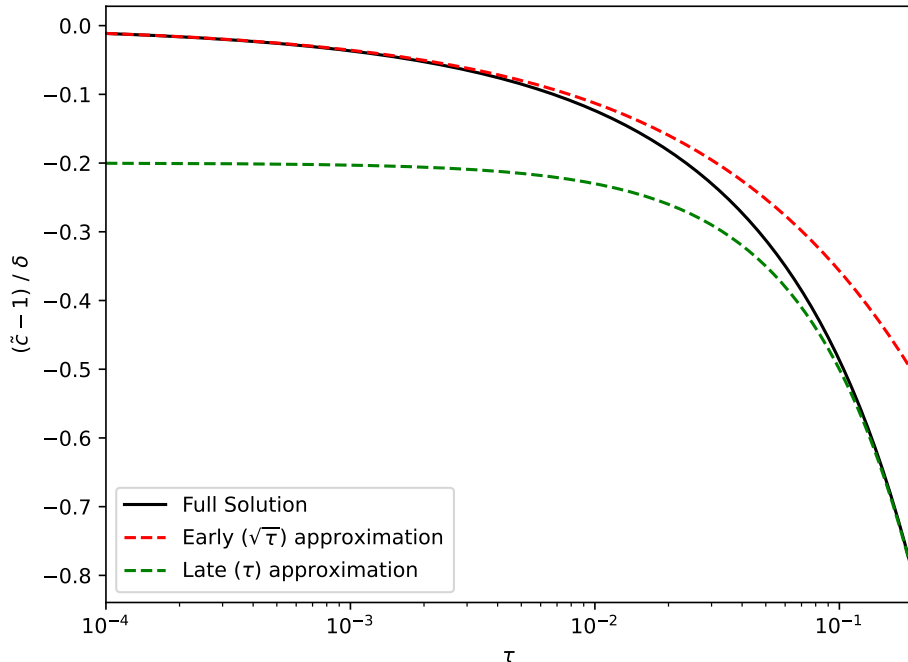


FIG. 6. Comparison of the full solution (solid black), the early $\sqrt{\tau}$ approximation (red dashed) and the late linear behaviour (green dashed).

To quantify the accuracy of the approximations, we calculate the relative error by

$$\text{Error}[\%] = 100 \times \frac{\tilde{c} - \tilde{c}_{\text{approx}}}{\tilde{c} - 1}, \quad (\text{A17})$$

where \tilde{c} is the exact solution while $\tilde{c}_{\text{approx}}$ is the approximation. The time dependence of the relative errors are presented in Figure 7. We see that the square-root solution (A13) is valid within 5% for $\tau < 0.0032$, 7.5% for $\tau < 0.0073$ and 10% for $\tau < 0.0132$.

On the other hand, we see the relative error in the late solution (A15) catches up with the early approximation (A13) at $\tau_{\text{eq}} = 0.0402$, with both errors at 17.25%. For $\tau > \tau_{\text{eq}}$, the linear approximation rapidly improves and the Sand equation is no longer applicable.⁶

In Figure 8 we demonstrate the effect of approximating the sphere as a semi-infinite slab using the GITT data for cathode delithiation from Ref.[23]. Here $\tau = tD/R^2$ is compute for each GITT pulse of duration t , with D inferred from the Sand equation. For this data, the value of τ is consistently above the 5% cutoff, occasionally going above the 7.5% line. The sand equation is valid within 10% accuracy in general. Even though GITT might not be accurate, it is still valid since τ stays below the critical τ_{eq} line, where Sand equation breaks down for spherical diffusion.

⁶ A typical value for the 5% accuracy of the linear solution is $\tau > 1.27$ [17, 22]. This actually corresponds to the accuracy associated with approximating $(\tilde{c} - 1)/\delta \approx -3\tau$. Instead, including the intercept $(\tilde{c} - 1)/\delta \approx -1/5 - 3\tau$, the linear behaviour becomes valid at a much earlier time, reaching 5% accuracy at $\tau > 0.0783$.

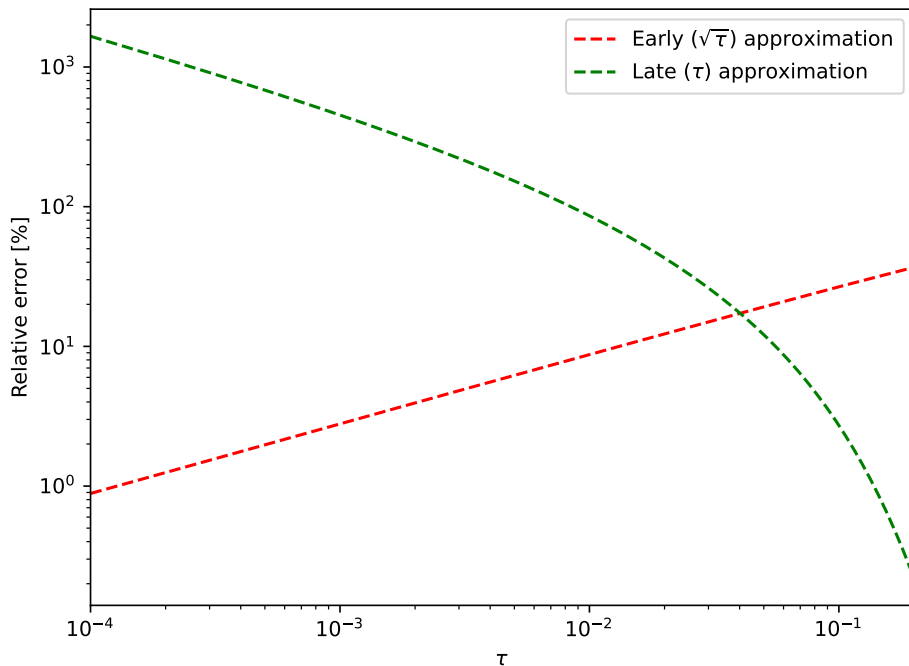


FIG. 7. Comparison of the full solution (solid black), the early $\sqrt{\tau}$ approximation (red dashed) and the late linear behaviour (green dashed).

On the other hand, given a relative error $\Delta c/c$ in concentration, Eq.(A14) implies that the relative error in diffusivity is

$$\frac{\Delta D}{D} = -2 \frac{\Delta c}{c}. \quad (\text{A18})$$

Since the early solution (A14) consistently underestimates the drop in concentration, this leads to an overestimation of diffusivity larger by a factor of 2. For instance, a 5% error in \tilde{c} would translate into a 10% error in D .

Appendix B: Optimisation scheme

In this appendix, we present the pseudocode for the optimisation algorithm.

procedure INFERD(Data, \mathcal{N} , N_iter, β)

Divide Data into \mathcal{N} partitions, (time: t_α , voltage V_α)

for each partition α from 1 to \mathcal{N} **do**

Calculate \hat{c}_α as the average c in partition α

Define local loss \mathcal{L}_α using t_α, V_α , as a function of D_α

Perform grid search to find D_α that minimises \mathcal{L}_α

Store pair $(\hat{c}_\alpha, \hat{D}_\alpha)$

end for

Construct $\hat{D}(c)$ as a piecewise linear function with knots at $(\hat{c}_\alpha, \hat{D}_\alpha)$

if overlaps are manageable (e.g. GITT) **then**

for iteration from 1 to N_iter **do**

for each partition α **do**

Estimate gradient of the quasi-global loss including 2β with respect to $\hat{D}(\hat{c}_\alpha)$ numerically

Update $\hat{D}(\hat{c}_\alpha)$

end for

end for

else (e.g. constant C/10)

for iteration from 1 to N_iter **do**

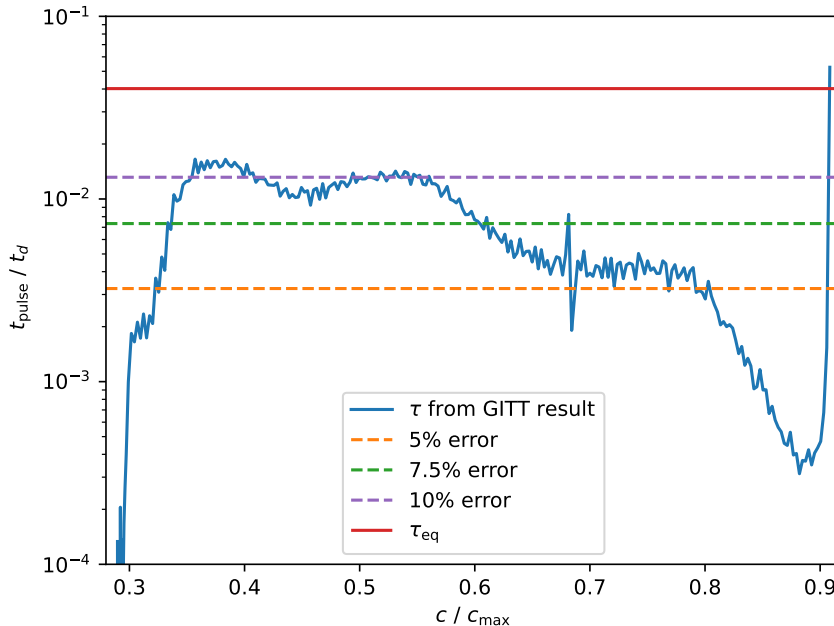


FIG. 8. Plot of the τ parameter for Chen et al [23] cathode delithiation data. The dashed orange, green and magenta lines denote the 5%, 7.5% and 10% accuracy lines, respectively. The solid red line corresponds to the critical τ_{eq} value above which, one cannot infer diffusivity from the Sand equation.

```

    Estimate gradients of global loss w.r.t each  $\hat{D}(\hat{c}_\alpha)$  numerically
    Update all  $\hat{D}(\hat{c}_\alpha)$  simultaneously
  end for
end if
end procedure

```

Appendix C: Determination of equilibrium potential using pOCV

The efficacy of ISDM, as with any inference technique, hinges on the accurate determination of the equilibrium potential $U_{eq}(c)$. In particular, if the output voltage differs from the correct U_{eq} once the system relaxed, the inference process becomes futile, yielding arbitrary outcomes.

When we are presented with a GIT data, it is straightforward to reconstruct the $U_{eq}(c)$ function from the voltages at the relaxation points. However, in order to make use of the flexibility of ISDM, it is crucial to find alternative approaches to determining $U_{eq}(c)$ without resorting to lengthy experimental techniques.

In this appendix, we outline the determination of the $U_{eq}^{(pOCV)}(c)$ function used in Sections IV and V. In order to construct the U_{eq} , we first note that

$$V_{\text{measured}} = U_{\text{eq}}(c_{\text{surf}}) \pm |\eta|, \quad (\text{C1})$$

where η is the reaction overpotential. The sign is positive (negative) during charging (discharging). Assuming a small enough current such that the charge is quickly dissipated across the particle, we can estimate the equilibrium potential as:

$$U_{\text{eq}} \approx \frac{1}{2} (V_{\text{charge}} + V_{\text{discharge}}), \quad (\text{C2})$$

such that the effect of the overpotential is cancelled. For the data set used in Sec. IV, which contains 10 charge and discharge cycles, we average over all 10 cycles, and show the estimated $U_{eq}^{(pOCV)}$ in Fig. 9, along with the $U_{eq}^{(\text{GITT})}$

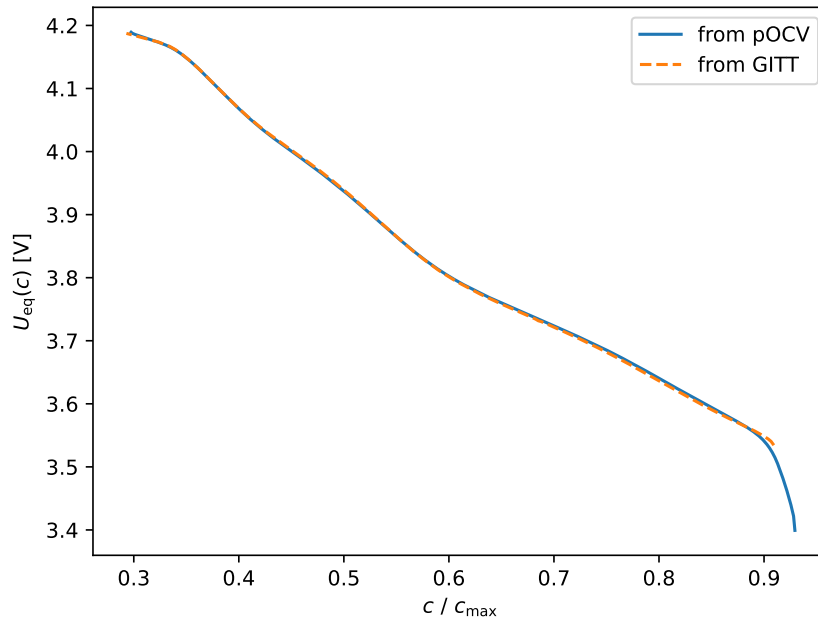


FIG. 9. The equilibrium potential estimated from pOCV data with constant $C/20$, compared to the one obtained directly from GITT data.

obtained from a full GITT charging cycle. The mean squared error between the two functions is 7×10^{-6} within the overlapping stoichiometry range.

-
- [1] M. Doyle, T. F. Fuller, and J. Newman, Modeling of galvanostatic charge and discharge of the lithium/polymer/insertion cell, *Journal of the Electrochemical Society* **140**, 1526 (1993).
 - [2] T. F. Fuller, M. Doyle, and J. Newman, Simulation and optimization of the dual lithium ion insertion cell, *Journal of the Electrochemical Society* **141**, 1 (1994).
 - [3] T. F. Fuller, M. Doyle, and J. Newman, Relaxation phenomena in lithium-ion-insertion cells, *Journal of the Electrochemical Society* **141**, 982 (1994).
 - [4] T. F. Fuller, M. Doyle, and J. Newman, Simulation and optimization of the dual lithium ion insertion cell, *J. Electrochem. Soc.* **141**, 1 (1994).
 - [5] A. Zülke, I. Korotkin, J. M. Foster, M. Nagarathinam, H. Hoster, and G. Richardson, Parametrisation and use of a predictive dfn model for a high-energy nca/gr-siox battery, *Journal of The Electrochemical Society* **168**, 120522 (2021).
 - [6] C. Schmitt, M. Gerle, D. Kopljar, and K. A. Friedrich, Full parameterization study of a high-energy and high-power li-ion cell for physicochemical models, *Journal of The Electrochemical Society* **170**, 070509 (2023).
 - [7] M. Ecker, T. K. D. Tran, P. Dechent, S. Käbitz, A. Warnecke, and D. U. Sauer, Parameterization of a physico-chemical model of a lithium-ion battery: I. determination of parameters, *Journal of The Electrochemical Society* **162**, A1836 (2015).
 - [8] M. Ecker, S. Käbitz, I. Laresgoiti, and D. U. Sauer, Parameterization of a physico-chemical model of a lithium-ion battery: II. model validation, *Journal of The Electrochemical Society* **162**, A1849 (2015).
 - [9] F. B. Planella, W. Ai, A. M. Boyce, A. Ghosh, I. Korotkin, S. Sahu, V. Sulzer, R. Timms, T. G. Tranter, M. Zyskin, S. J. Cooper, J. S. Edge, J. M. Foster, M. Marinescu, B. Wu, and G. Richardson, A continuum of physics-based lithium-ion battery models reviewed, *Progress in Energy* **4**, 042003 (2022).
 - [10] S. J. Moura, F. B. Argomedo, R. Klein, A. Mirtabatabaei, and M. Krstic, Battery state estimation for a single particle model with electrolyte dynamics, *IEEE Transactions on Control Systems Technology* **25**, 453 (2016).
 - [11] M. Guo, G. Sikha, and R. E. White, Single-particle model for a lithium-ion cell: Thermal behavior, *Journal of The Electrochemical Society* **158**, A122 (2010).
 - [12] S. G. Marquis, V. Sulzer, R. Timms, C. P. Please, and S. J. Chapman, An asymptotic derivation of a single particle model with electrolyte, *Journal of The Electrochemical Society* **166**, A3693 (2019).
 - [13] G. Richardson, I. Korotkin, R. Ranom, M. Castle, and J. Foster, Generalised single particle models for high-rate operation of graded lithium-ion electrodes: Systematic derivation and validation, *Electrochimica Acta* **339**, 135862 (2020).

- [14] A. A. Wang, S. E. J. O’Kane, F. B. Planella, J. L. Houx, K. O’Regan, M. Zyskin, J. Edge, C. W. Monroe, S. J. Cooper, D. A. Howey, E. Kendrick, and J. M. Foster, Review of parameterisation and a novel database (liiondb) for continuum li-ion battery models, *Progress in Energy* **4**, 032004 (2022).
- [15] H. J. Sand, Iii. on the concentration at the electrodes in a solution, with special reference to the liberation of hydrogen by electrolysis of a mixture of copper sulphate and sulphuric acid, *The London, Edinburgh, and Dublin Philosophical Magazine and Journal of Science* **1**, 45 (1901).
- [16] W. Weppner and R. A. Huggins, Determination of the kinetic parameters of mixed-conducting electrodes and application to the system Li_3Sb , *J. Electrochem. Soc* **124**, 43 (1977).
- [17] A. Nickol, T. Schied, C. Heubner, M. Schneider, A. Michaelis, M. Bobeth, and G. Cuniberti, Gitt analysis of lithium insertion cathodes for determining the lithium diffusion coefficient at low temperature: Challenges and pitfalls, *Journal of The Electrochemical Society* **167**, 090546 (2020).
- [18] T. Kim, W. Choi, H.-C. Shin, J.-Y. Choi, J. M. Kim, M.-S. Park, and W.-S. Yoon, Applications of voltammetry in lithium ion battery research, *Journal of Electrochemical Science and Technology* **11**, 14 (2020).
- [19] G. Leftheriotis, S. Papaefthimiou, and P. Yianoulis, Dependence of the estimated diffusion coefficient of Li_2WO_3 films on the scan rate of cyclic voltammetry experiments, *Solid State Ionics* **178**, 259 (2007).
- [20] C. Ho, I. D. Raistrick, and R. A. Huggins, Application of a-c techniques to the study of lithium diffusion in tungsten trioxide thin films, *Journal of The Electrochemical Society* **127**, 343 (1980).
- [21] C. J. Wen, B. A. Boukamp, R. A. Huggins, and W. Weppner, Thermodynamic and mass transport properties of “LiAl”, *Journal of The Electrochemical Society* **126**, 2258 (1979).
- [22] Y.-C. Chien, H. Liu, A. S. Menon, W. R. Brant, D. Brandell, and M. J. Lacey, Rapid determination of solid-state diffusion coefficients in li-based batteries via intermittent current interruption method, *Nature communications* **14**, 2289 (2023).
- [23] C.-H. Chen, F. B. Planella, K. O’Regan, D. Gastol, W. D. Widanage, and E. Kendrick, Development of experimental techniques for parameterization of multi-scale lithium-ion battery models, *Journal of The Electrochemical Society* **167**, 080534 (2020).
- [24] Y. Zeng, P. Albertus, R. Klein, N. Chaturvedi, A. Kojic, M. Z. Bazant, and J. Christensen, Efficient conservative numerical schemes for 1d nonlinear spherical diffusion equations with applications in battery modeling, *Journal of The Electrochemical Society* **160**, A1565 (2013).
- [25] The E. Kendrick group, Birmingham University, unpublished data.
- [26] I. Korotkin, S. Sahu, S. E. J. O’Kane, G. Richardson, and J. M. Foster, Dandelion v1: An extremely fast solver for the newman model of lithium-ion battery (dis)charge, *Journal of The Electrochemical Society* **168**, 060544 (2021).
- [27] H. S. Carslaw and J. C. Jaeger, *Conduction of heat in solids*, 2nd ed. (Oxford University Press, London, England, 1959).
- [28] V. R. Subramanian and R. E. White, New separation of variables method for composite electrodes with galvanostatic boundary conditions, *Journal of Power Sources* **96**, 385 (2001).
- [29] N. Liron, Some infinite sums, *SIAM Journal on Mathematical Analysis* **2**, 105 (1971), <https://doi.org/10.1137/0502010>.